Biointerface Research in Applied Chemistry
Open-Access Journal (ISSN: 2069-5837)

Article
Volume 13, Issue 1, 2023, 60
https://doi.org/10.33263/BRIAC131.060

Magnetic ZnO/CdO Nanocomposite for Effective Drug Delivery System for Cancer Therapy

Hanan H. Mohamed [1,*], Tamer E. Youssef [2], Doaa Abdel Fadeel [3]

[1] Chemistry Department, Faculty of Science, Helwan University, Ain Helwan, Cairo, 11795, Egypt; m_h_hanan_0503@yahoo.com (H.H.M.);
[2] Applied Organic Chemistry Department, National Research Centre, Dokki, Cairo 12622, Egypt; Tamezzat@yahoo.com (T.E.Y.);
[3] Pharmaceutical Technology Unit, Department of Medical Applications of Laser, National Institute of Laser Enhanced Sciences, Cairo University, Giza, Egypt; doaa.fadeel@niles.edu.eg (D.A.F.);
* Correspondence: m_h_hanan_0503@yahoo.com (H.H.M.);

Scopus Author ID 55172120500
Received: 20.11.2021; Accepted: 19.12.2021; Published: 30.01.2022

Abstract: ZnO, ZnO/CdO, and Magnetic Ni-ZnO/CdO nanocomposite have been eco-friendly synthesized using Black Rice Husk Extract (BRHE) and water instead of hazardous chemicals and solvents. The anticancer drug Doxorubicin (Dox) was loaded on the PVA-coated biomimetic nanomaterials. The successful synthesis of the pure nanomaterials and the Dox-nanomaterial systems has been confirmed by evaluating their structural, crystalline, textural, surface, and optical properties using various characterization techniques. The Dox-nanomaterials systems were used as anticancer drugs against HEPG2 cells as a model of human cancerous cells. The *in vitro* Dox release was slower and more sustained from Ni-ZnO/CdO composite compared to the other individual nanomaterials, suggesting that a hydrogen bond strongly attached more Dox molecules to the surface Ni-ZnO/CdO. Moreover, the cytotoxicity investigations on the HEPG2 cell line showed that higher toxicity was obtained by Ni-doped nanocomposite, consistent with the results of *in vitro* release. This study provides novel magnetic Nanocarriers that can be used as anticancer drug delivery systems after more *in vivo* investigations on animals or clinical investigations.

Keywords: magnetic Ni- ZnO/CdO; green synthesis; doxorubicin; anticancer drug delivery; HEPG2 cell.

1. Introduction

Semiconductor metal oxide nanoparticles attracted great attention in biomedical applications such as drug delivery, cancer therapy, and technological applications such as optical and nanoelectronic devices and photocatalysis [1, 2]. It has been found that metal oxide nanoparticles can kill cancer cells in low concentrations. Zinc oxide (ZnO) nanoparticles have potential in cancer therapy due to their ability to induce cancer cell apoptosis [3]. In addition, cadmium oxide (CdO) nanoparticles were found to be an efficient metal oxide nanomaterial for cancer therapy via destruction of the cancer cell wall and the interaction with DNA causing protein damage [4]. Interestingly, CdO nanoparticles were found to be not dangerous for human and mammalian cells. CdO coupled ZnO with well-defined morphology may enhance the anticancer activity in a better way.

Moreover, magnetic nanoparticles have attracted considerable attention in the field of drug delivery. Anticancer drugs are known for their non-selectivity, affecting healthy and non-healthy tissues. One of the approaches to diminish the undesirable effects is to load these drugs to magnetic nanoparticles, subjecting the target tissue to a magnetic field. This will lead to selective accumulation of the nanoparticles in the desired site of action. The temperature will be increased at the tumor site, leading to selective destruction of tumor tissue [5, 6]. However, magnetic nanoparticles are recognized by the reticuloendothelial system and rapidly removed from the blood circulation [7]. Hydrophilic polymers usually coat nanoparticles to elongate their presence in circulation and provide additional functional groups that facilitate interaction with various drugs allowing the use of nanoparticles as powerful drug delivery systems [8].

Nanomaterials-based cancer therapy can be enhanced by utilizing a combination of nanomaterials and anticancer drugs, leading to higher tumor control and reducing undesired side effects [9]. Combination therapy can thus overcome cross-resistance and achieve synergistically enhanced therapeutic outcomes without significantly increasing toxicities.

Various chemical and physical methods have been reported to synthesize metal oxide nanoparticles, such as sol-gel, precipitation, solvothermal and hydrothermal methods. However, the chemical method for nanoparticles synthesis consumes hazardous chemicals and toxic solvents as well as involves high energy consumption. Recently, green methods for nanomaterials synthesis have attained great attention. In green methods, plant/plant waste extracts can be utilized as reducing/oxidizing agents, as well as capping agents [10-12].

In the present study, magnetic Ni-ZnO/CdO nanocomposite has been synthesized by a green method using plant extract. The synthesized nanomaterials were coated by a hydrophilic polymer polyvinyl alcohol (PVA) which is frequently used for nanoparticles coating due to its high biocompatibility and stability [13]. The properties of the prepared nanocomposite and its individual components (i.e., ZnO, CdO, ZnO/CdO) have been evaluated by various techniques.

Doxorubicin (Dox) was chosen as a model of cytotoxic drug that is FDA approved for the treatment of several types of cancer. Though Dox is one of the most potent anticancer drugs, its clinical use is hampered by its severe cardio- and nephrotoxicity. Moreover, cancerous cells can easily develop drug resistance against Dox due to poor cellular uptake and rapid drug release. So, loading Dox to nanoparticles has attracted significant attention in recent research to maximize its targeting to tumor tissue and minimize its effects on healthy ones [14, 15]. The anticancer activity of pure and DOX loaded to the PVA coated nanomaterials has been tested as an anticancer drug against HEPG2 cells as a model of human cancerous cells. However, there are no reports on using such a composite of magnetic nanomaterials for anticancer activity to the best of our knowledge.

2. Materials and Methods

2.1. Materials.

Methanol, zinc acetate dihydrate, nickel acetate tetrahydrate, cadmium acetate dehydrate, Polyvinyl alcohol (PVA), dimethyl sulphoxide (DMSO), and methyl thiazolyl diphenyl- tetrazolium bromide (MTT) were purchased from Sigma Aldrich. Doxorubicin hydrochloride (Dox, Adricin®) is a product of EIMC united Pharmaceuticals (Badr city, Cairo, Egypt). Hepatocellular carcinoma cell line (HepG2) was purchased from American tissue culture collection through VACSERA, Cairo, Egypt. Roswell Park Memorial Institute medium

(RPMI) was purchased from Sigma Aldrich. Fetal bovine serum (FBS), penicillin and streptomycin were purchased from Lonza, Belgium.

2.2. Materials preparation of Black Rice Husk Extract (BRHE.)

The Black Rice Husk was provided from a local paddy mill in El Gharbia, Egypt. It was washed with distilled water and then dried under the sun, then ground to a fine powder. The extraction of BRH is performed by a soxhlet extraction method using methanol as a solvent. Methanol was removed using a rotary evaporator under vacuum conditions to obtain a reddish-brown solid of BRHE.

2.3. Eco-Friendly Synthesis of ZnO, CdO, ZnO/CdO, and Ni-ZnO/CdO.

The pure ZnO nanoparticles were synthesized via sonochemical method using zinc acetate dihydrate ($Zn(CH_3COO)_2 \cdot 2H_2O$, ≥99.0), as a ZnO precursor, and Rice Husk extract (RHE). In a typical synthesis, aqueous BRHE solution (1 g, 100 ml) was gradually added to an aqueous solution of zinc acetate (2 g, 100 ml) under ultrasonic irradiation (USC200T, VWR International; 45 kHz, 60 W). The resulted suspension was further sonicated for 4 h. Pure CdO nanoparticles were synthesized by the same method mentioned above using cadmium acetate dihydrate ($Cd(CH_3COO)_2 \cdot 2H_2O$, ≥98.0) as a CdO precursor. ZnO/CdO nanocomposites were synthesized by dissolving the desired amount of ZnO and CdO (ZnO:CdO = 1:2) in distilled water followed by drop-wise adding 100 mL of BRHE under ultrasonication. After ultrasonic treatment, the solid products were separated, washed by distilled water, and then dried at 70°C for 1hr. Calcination at 500 ºC for 1 h was applied to remove any organic residue from the plant extract. To enhance the magnetic properties, nickel-doped ZnO/CdO nanocomposite was synthesized by the same method of un-doped ZnO/CdO but in the presence of 10 % Ni(II) using nickel acetate tetrahydrate ($Ni(OCOCH_3)_2 \cdot 4H_2O$). According to the previous work, it is proposed that the compounds in aqueous BRH extract can act as precipitating and directing agents during the synthesis process of ZnO and CdO nanomaterials [10-12].

The synthesized nanoparticles were then coated by PVA, as Kayal and Ramanujan (2010) described with slight modification [16]. Briefly, a solution of PVA in distilled water (2 mg/ml) was prepared at 55°C. The synthesized nanoparticles were then added to PVA solution under continuous stirring at 400 rpm for 24 h, the concentration of PVA was adjusted to be 5% by weight.

2.4. Loading of Dox to PVA-coated nanoparticles.

For loading Dox, 300 µl Dox solutions (2mg/mL) were added to 2.5 ml PVA-coated nanoparticles. The Dox: nanoparticle ratio was kept at 1:10. The solutions were kept under continuous stirring at 400 rpm for 6h. The obtained Dox-PVA nanoparticles were finally separated by centrifugation at 5000 rpm (Centrikon T-42 K, Kontron Instruments, UK) for 10 min and left in the open air to dry. To determine the encapsulation efficiency (E.E%), the concentration of Dox in the supernatants was measured spectroscopically using UV-VIS double beam spectrophotometer (Rayleigh UV-2601). The absorbance was measured at 489 nm, and the Dox concentration was calculated from a standard curve. The encapsulation efficiency was calculated [17] as follows:

[(Initial Dox concentration - Dox concentration in the supernatant)/ initial Dox concentration] X100.

2.5. Materials characterization.

XRD measurements were performed using a Cu-K x-ray with tube conditions of 40 kV. SEM measurement was carried out by using TESCAN (VEGA3). TEM analysis was performed on TEM FEI, Morgagni 268, Brno, Czech Republic. UV-vis diffuse reflectance measurements have been performed on Shimadzu UV4100 spectrometer, and UV–Vis absorption measurements were recorded on UV-Vis Spectrophotometer-UVD-3200, LABOMED. To confirm the polymer coating and the drug loading, FTIR was conducted to free PVA, free Dox, and Dox-loaded PVA- coated nanoparticles. The spectra were recorded using JASCO, FT/IR-4100 type A. Magnetic hysteresis loop at room temperature was measured using a VSM (Microsense EZ9) having a maximum magnetic field strength of 22.5 kOe. The Zeta potential of PVA-coated nanoparticles unloaded and loaded by Dox was measured by zeta sizer (Malveran instrument Ltd, UK).

2.6. In vitro drug release.

The release behavior of Dox from nanoparticles was studied throughout 24h at acidic pH under sink conditions. 1 mL of each Dox loaded PVA coated nanoparticles (equivalent to 240 µg Dox) was placed in a dialysis bag membrane (molecular weight cut off 12,000–14,000), presoaked in the acceptor medium for 24h. The dialysis membranes were suspended in 100 ml PBS buffer (pH 5.4) to simulate the acidic environment of tumor cells. The solutions were kept at 37ºC under continuous stirring. Aliquots of 1 mL were withdrawn at predetermined time intervals and replaced by a fresh medium to maintain the sink conditions. The concentration of Dox in the withdrawn aliquots was measured spectroscopically at 489 nm, as mentioned above.

2.7. Cytotoxicity study on HEPG2 cell line.

2.7.1. Cytotoxicity of PVA-coated nanoparticles.

The cytotoxicity of the PVA-coated nanoparticles was assessed on the HEPG2 liver carcinoma cell line by MTT assay. Briefly, HepG2 cells were seeded in flat-bottomed 96-well culture plates. Each well was seeded by 1×10^4 cells in 100 µL growth media (RPMI) containing 10% deactivated FBS, 100 units/mL penicillin, and 100 µg/mL streptomycin.

The cells were incubated at 37°C, in a humidified atmosphere containing 5% carbon dioxide for 24 h to adhere to the wells. The cells were further incubated for 24 h at 37 °C after being treated with different concentrations of PVA, PVA-ZnO, PVA ZnO/CdO, and PVA Ni-ZnO/CdO. Some cells were incubated in the growth media without any treatment to serve as a control. Afterward, 100 µL of medium containing 20 µL MTT in phosphate buffer (5 mg/ml) was added to each well, and the plates were incubated for a further 3h at 37 ºC. The MTT was removed by washing three times with phosphate-buffered saline (PBS), and the formed formazan crystals were dissolved in 200 µL DMSO. The absorbance of the solutions was immediately recorded at 570 nm using a microplate reader (Biotek Instrument, EL800). The % cell viability relative to the control wells containing cell culture medium without the samples was calculated as follows [17]:

$$\%\ Cell\ Viability = \frac{Absorbance\ at\ 570\ nm\ of\ test\ cells}{Absorbance\ at\ 570\ nm\ of\ control\ cells} \times 100$$

2.7.2. Cytotoxicity of Dox-loaded-PVA-coated nanoparticles.

The cells were seeded with the same procedure. Afterward, they are treated with aqueous Dox solution, and Dox loaded PVA coated ZnO, ZnO/CdO, and Ni-ZnO/CdO, at a Dox concentration of 20 µg/mL. 24h later, MTT assay was carried out, and the cell viability for all tested samples was calculated as described above.

3. Results and Discussion

3.1. Characterization of BRHE.

XRD pattern of the BRHE is shown in Figure 1 (a). A band at 20.8° is observed to be attributed to crystalline organic compounds in the BRHE. FTIR spectrum of the obtained BRHE is shown in Figure 1 (b) with a peak around 3400 cm^{-1}, which is mainly attributed to O-H and N-H stretching vibration, while the peak at ~2350 cm^{-1} can be due to C-H stretching vibration. Aromatic C=C stretching vibration can be confirmed from the two peaks around 1610 and 1750 cm^{-1}. The results confirm the presence of antioxidants and phenolic compounds in BRHE [18, 19].

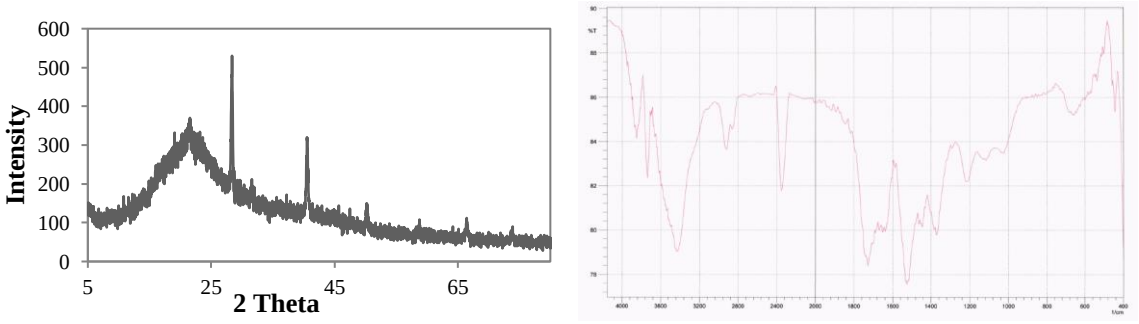

Figure 1. (**a**) XRD pattern and (**b**) FTIR spectrum of the Rice Husk Extract.

3.2. Characterization of nanomaterials.

The XRD patterns of the green synthesized nanomaterials are shown in Figure 2. The XRD pattern of pure ZnO shows the typical bands assigned to wurtzite ZnO (JPCDS 36-1451) [20, 21]. The XRD pattern of pure CdO shows peaks at 2θ=32.8°, 38.18°, 55.1°, 65.8° and 69.4° assigned to the cubic crystalline CdO (JCPDS data card no.05-0640) [22]. The diffraction pattern of ZnO/CdO nanocomposite shows the typical bands of ZnO along with bands of CdO. The XRD pattern of Ni-doped ZnO/CdO nanocrystals shows no changes compared to un-doped ZnO/CdO nanocomposite, confirming that no additional phase of NiO has been formed. The high-intensity peaks at (111) and (200) of Ni-ZnO/CdO indicate the substitution of Ni (II) ion with smaller ionic radius to Cd (II) sites.

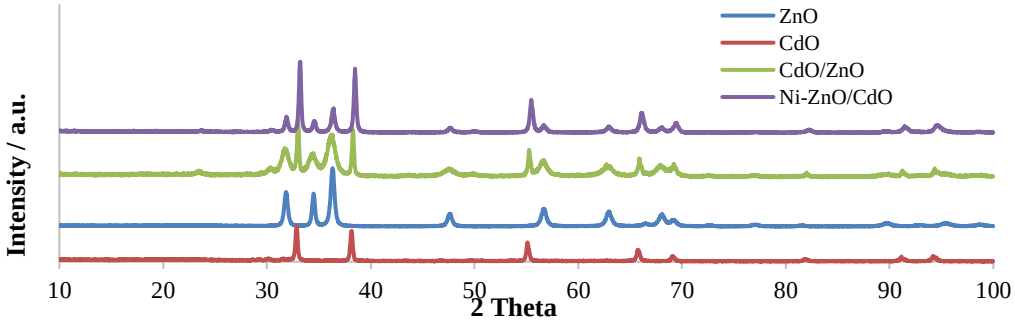

Figure 2. XRD patterns of the as-synthesized pure ZnO, pure CdO, ZnO/CdO, and Ni-doped ZnO/CdO nanocomposites.

The diffuse reflectance spectra of samples (Figure 3 (a)) includes ZnO with absorption in the UV region at 380 nm. The spectrum of CdO shows the absorption of CdO in the visible region with an absorption edge of about 500 nm. ZnO/CdO nanocomposite shows more response to visible light than pure ZnO, which can be ascribed to the electronic interaction among ZnO/CdO. The absorption of Ni-doped ZnO/CdO nanocomposite has been further improved toward visible light absorption. The bandgap energies of all nanomaterials have been analyzed using the Kubelka-Munk relation (Figure 3 (b)). The obtained bandgap energy of the pure green ZnO and CdO nanoparticles has been estimated to be (3.15 eV) and (1.8 eV), respectively, which are found to be in good agreement with the reported values [20, 22]. ZnO/CdO nanocomposites exhibited two absorption edges at 2.9 and 1.5 eV, respectively, due to the cooperative light absorption by ZnO and CdO. Similar results were obtained for Ni-ZnO/CdO nanocomposite with absorption bandgap at 2.65 and 1.4 eV with redshift to the un-doped nanocomposite for ZnO and CdO, respectively. The shift of the bandgap energies is attributed to the additional energy levels by the dopant.

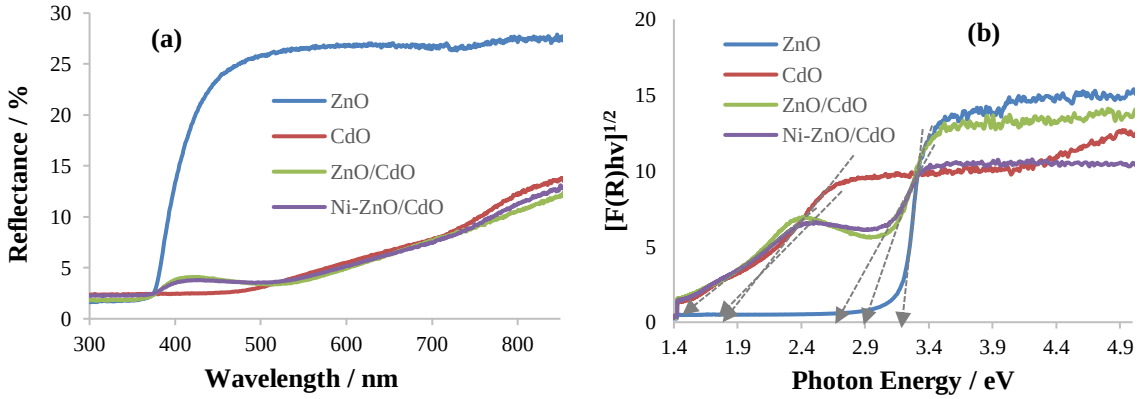

Figure 3. (**a**) UV-vis diffuse reflectance spectra of the as-synthesized pure ZnO, pure CdO, ZnO/CdO, and Ni-ZnO/CdO nanocomposites and (**b**) corresponding Kubelka-Munk plots.

The FTIR spectra of all materials are shown in Figure 4. The FTIR spectrum of ZnO shows a band at 439 cm^{-1}, which is assigned to Zn-O stretching vibration, and a broadband at 3435 cm^{-1} due to the surface OH group starching vibration [20, 21]. The FTIR spectrum of CdO nanoparticles shows weak vibrational bands at 3442, 1747, and 1371 cm^{-1}, which are mainly attributed to the stretching and bending vibration of hydroxyl surface adsorbed water molecules.

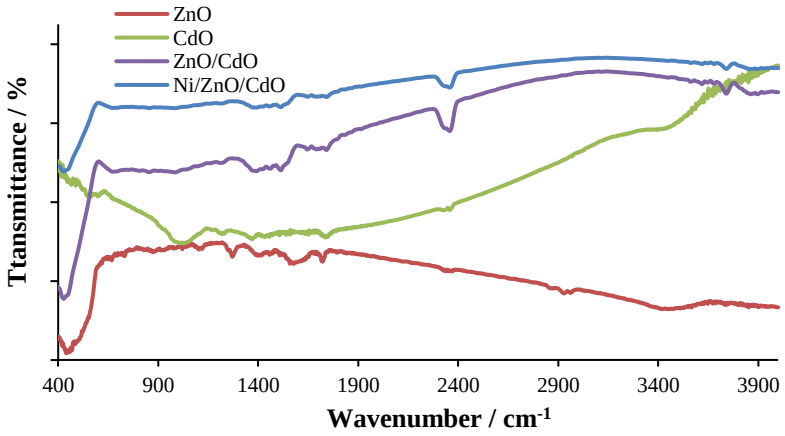

Figure 4. FTIR spectra of the as-synthesized pure ZnO, pure CdO, ZnO/CdO, and Ni-ZnO/CdO nanocomposites.

The broadband acquired at 430-555 cm^{-1} can be assigned to Cd-O stretching vibration of CdO nanoparticles [22]. FTIR spectra of ZnO/CdO nanoparticles showed the broadband at 3435 cm^{-1}, which is assigned to stretching vibration of (O-H) in addition to the main characteristic functional group of Cd-O and Zn-O at 426 cm^{-1}. The two peaks at 2350 and 2330 cm^{-1} indicate the stretching of the O=C=O bond due to the presence of CO_2 in the atmosphere [23]. The FTIR spectrum of Ni-doped ZnO/CdO is identical to that of un-doped ZnO/CdO nanocomposite, indicating that doping does not affect the bonding environment of the un-doped composite.

M-H curves (at 300 K) (Figure 5) clearly show the typical week ferromagnetic (FM) saturation behavior of Ni-ZnO/CdO sample with saturation magnetization of 8×10^{-3} emu/gm. There are two possibilities for the existence of ferromagnetism in Ni-ZnO/CdO, either due to the clustering of metallic nickel for which intrinsic ferromagnetism rises from the charge carriers or can be attributed to oxygen vacancies, size effect, and exchange interaction between doped transition metal ion and oxygen ion spins [24, 25].

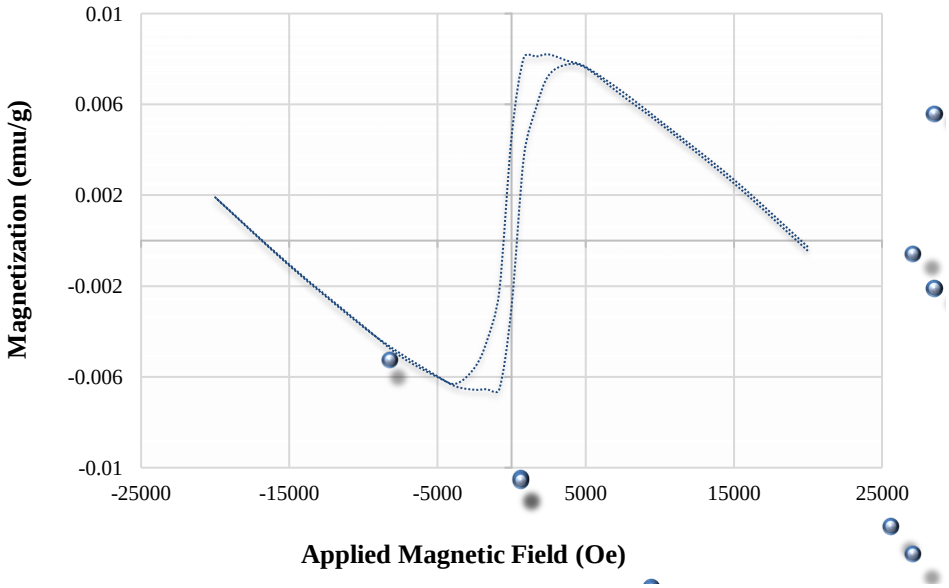

Figure 5. M-H loop of Ni-ZnO/CdO nanocomposite.

SEM images of the synthesized nanomaterials show agglomerated uniformly shaped particles. SEM image of CdO (Figure 6 (a)) shows smaller particles while bigger particles was obtained for ZnO (Figure 6 (b)), nanocomposites ZnO/CdO and Ni-ZnO/CdO (Figure 6 (c) and (d)). TEM images show agglomeration of nearly spherical particles, and distorted hexagonal were observed for ZnO and CdO, respectively (Figure 7). In addition, CdO/ZnO nanoparticles showed distorted hexagonal morphology with sizes ranging from 60-70 nm in addition to the presence of smaller CdO particles. The images of Ni-doped ZnO/CdO are found to be similar to the un-doped nanocomposite.

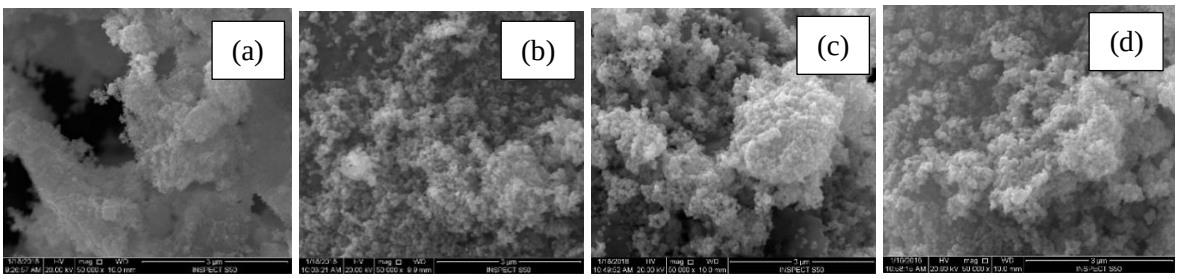

Figure 6. SEM images of (**a**) pure CdO, (**b**) pure ZnO, (**c**) ZnO/CdO and (**d**) Ni-ZnO/CdO nanocomposites.

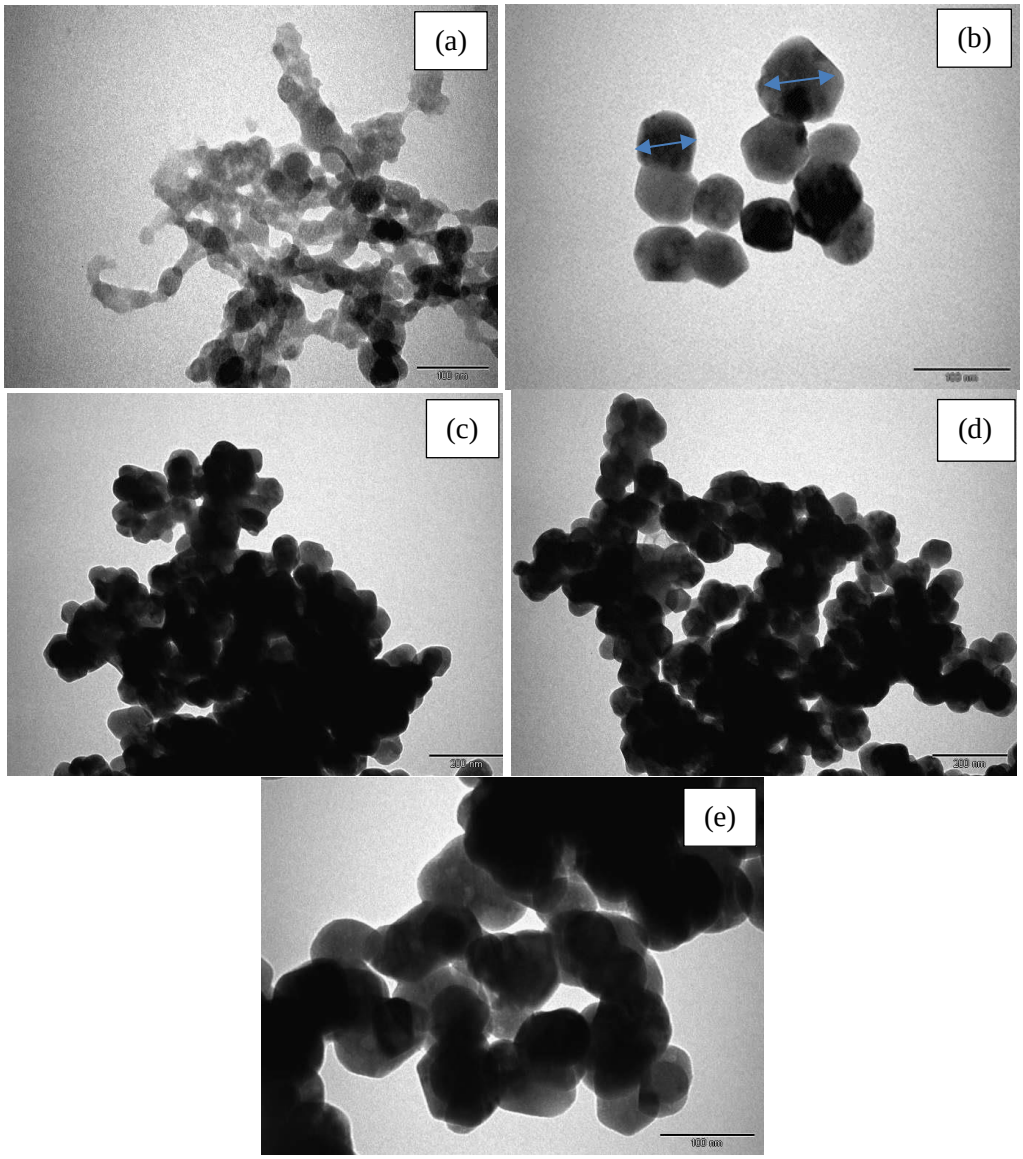

Figure 7. TEM images of (**a**) pure CdO, (**b**) pure ZnO, (**c**) ZnO/CdO and (**d, e**) Ni-ZnO/CdO nanocomposites.

3.3. Loading Dox on different PVA-coated nanoparticles.

Dox was successfully loaded on different PVA-coated nanoparticles with a relatively high encapsulation efficiency of 69±2 % and 94±3.1 % in the case of PVA-ZnO and PVA-ZnO/CdO, respectively. Furthermore, the encapsulation efficiency was further improved for PVA-Ni-ZnO/CdO to achieve nearly 100 %. This very high E.E may be attributed to the high electrostatic interaction between the Dox, and the PVA coated particles, as further confirmed by zeta potential and FTIR.

PVA coated ZnO, ZnO/CdO, and Ni- ZnO/CdO exhibited negative zeta potential of -14, -19, and -13 mV, respectively, due to the presence of negative hydroxyl group of the PVA polymer [26]. After Dox loading, the zeta potential of ZnO, ZnO/CdO became positive (6 and 17 mV, respectively), while that of Ni-ZnO/CdO remained negative but decreased to -7. The decrease in negative charge indicates the loading of positive Dox molecules to the nanoparticle surface by electrostatic interaction [27].

The FTIR of pure DOX (Figure 8) shows peaks at 3447 cm^{-1} due to N-H stretching vibrations for the primary amine structure and a peak at 1638 cm^{-1} due to N-H bending vibration. The FTIR spectrum of PVA shows a large band at 3432 cm^{-1}, which is attributed to the stretching O–H from hydrogen bonds, the band at 2931 cm^{-1} due to the alkyl groups C–H

stretching vibration, and the band at 1713 cm^{-1} is due to the C–O stretching vibration of acetate group in PVA [28, 29].

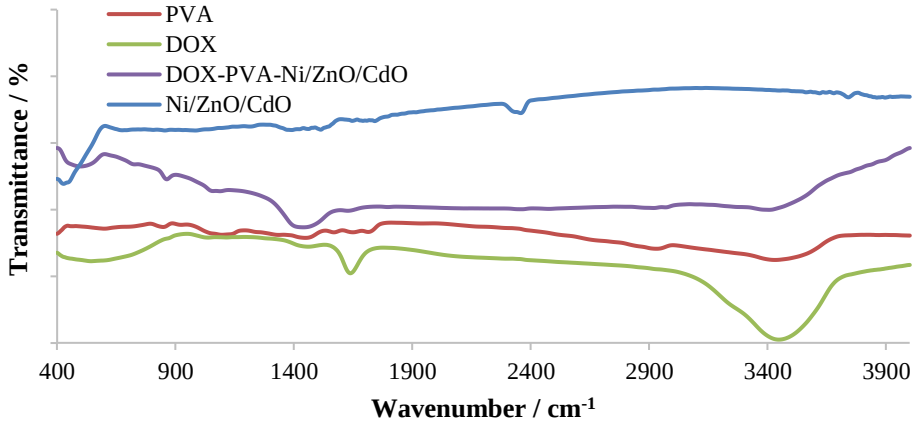

Figure 8. FTIR spectra of the DOX loaded PVA coated Ni-ZnO/CdO.

In the FTIR spectrum of DOX loaded on PVA-coated nanoparticles, peaks due to N–H stretching vibrations and O–H vibrations are broadened and shifted to lower frequency (3406 cm^{-1}). In addition, the band at 1638 cm^{-1} due to DOX N-H bending vibration diminishes in the FTIR spectrum of DOX-loaded PVA-nanoparticles. The results revealed that attachment of DOX to the PVA coated nanoparticles occurs via the hydrogen bonding of $–NH_2$ and –OH groups of DOX with –OH groups of PVA.

3.4. In vitro drug release.

Dox exhibited initial burst release followed by sustained release (Figure 9) over a period of 24 h. After 6 h, 83% and 80% were released from Dox-ZnO and Dox-ZnO/CdO, respectively, while only 55% was released from Dox-Ni-ZnO/CdO. After 24 h, 91%, 90% and 82% was released from Dox-ZnO, Dox-ZnO/CdO and Dox-Ni-ZnO/CdO, respectively. These results revealed that the Dox could be readily released from the synthesized nanoparticles in the slightly acidic microenvironment of tumor cells, consistent with many previous studies [30, 31]. Dox molecules that are weekly adsorbed on the surface of the nanoparticles are released first, causing initial fast release followed by sustained release of the strongly attached molecules [31]. The release of Dox was slower and more sustained from Ni-ZnO/CdO, suggesting that more Dox molecules were strongly attached by a hydrogen bond to the surface of Ni-ZnO/CdO.

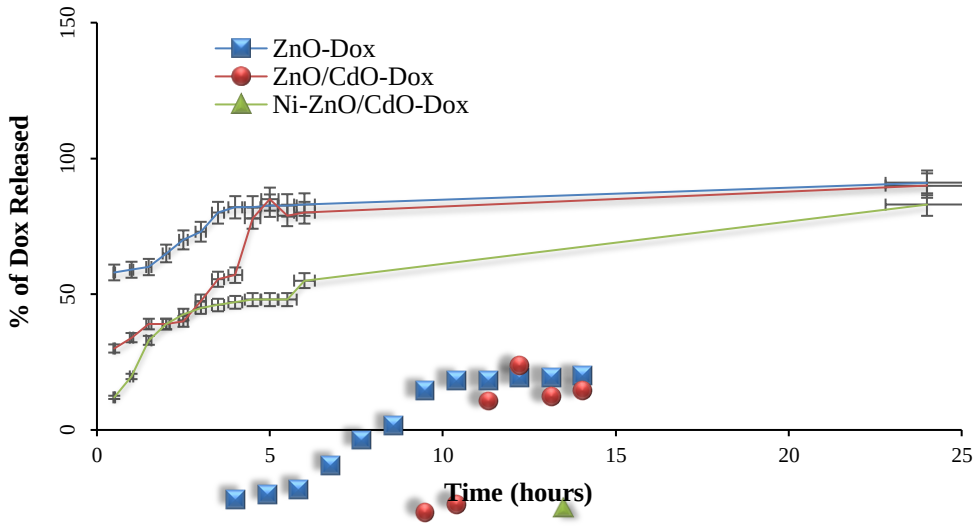

Figure 9. *In vitro* release behavior of Dox from different nanomaterials.

3.5. Cytotoxicity measurements.

The cytotoxicity of the synthesized nanoparticles was tested by MTT reduction assay on the HEPG2 cell line as a model of human cancerous cells.

Figure 10 illustrates the cytotoxicity of PVA, PVA-ZnO, PVA-ZnO/CdO, and PVA-Ni-ZnO/CdO at different concentrations. PVA was found to be nontoxic at all tested concentrations. All the tested nanoparticles were found to have no or very low cytotoxicity at low concentrations (10 µg/mL). However, at higher concentrations (100 µg/mL), PVA-Ni-ZnO/CdO was the most cytotoxic among the tested materials. At a very high concentration (700 µg/mL), no significant difference was observed between tested nanomaterials ($p>0.05$). Cell viability of 30%, 22%, and 25% was obtained for ZnO, ZnO/CdO, and Ni-ZnO/CdO, respectively. The cytotoxicity of ZnO nanoparticles on HEPG2 cells may be due to DNA fragmentation and the generation of reactive oxygen species [32].

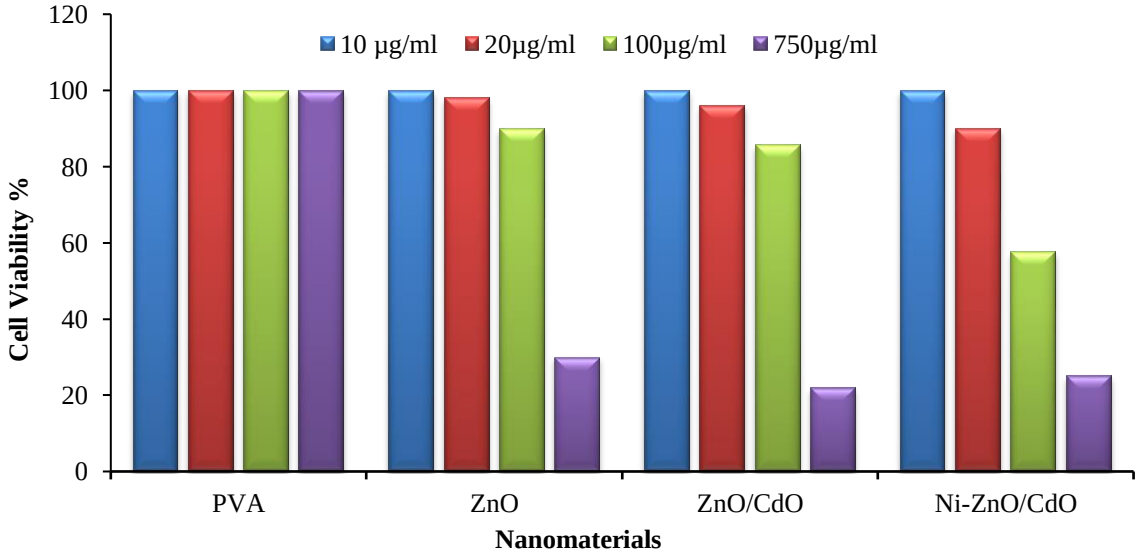

Figure 10. Cytotoxicity of PVA and PVA-coated nanoparticles at different concentrations.

Cytotoxicity of Dox loaded to different PVA-coated nanoparticles is illustrated in Fig. 11. The cells are incubated for 24 h with different Dox-loaded nanoparticles and a free Dox aqueous solution, all equivalent to 20 µg/mL Dox. Aqueous Dox solution did not affect cell viability when used in a concentration of 20 µg/mL. This may be attributed to the drug

resistance developed by cancerous cells; consequently, high drug doses are required to impart cytotoxicity [31]. However, higher concentrations are avoided as they can cause severe cardiotoxicity in clinical practice [33].

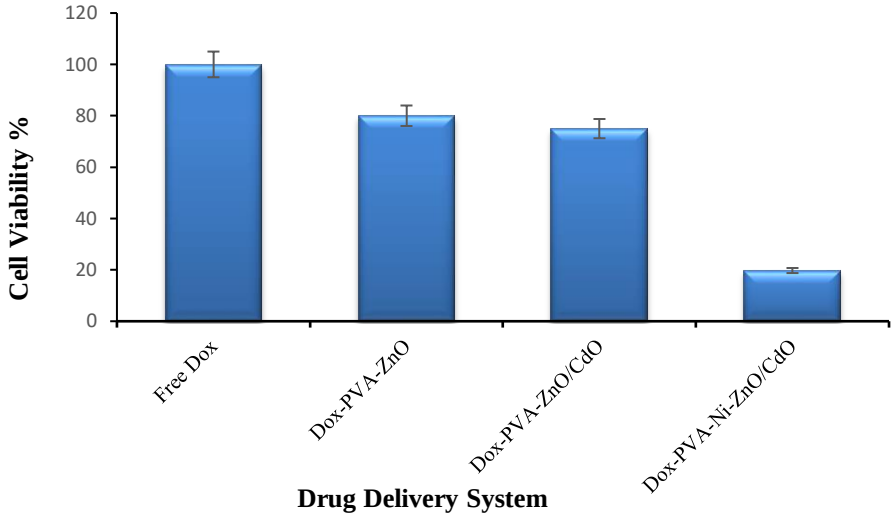

Figure 11. Cytotoxicity of Aqueous free Dox and different Dox-loaded nanoparticles (all equivalent to Dox concentration of 20 µg/mL).

About 80 % and 75 % cell viability were obtained in the case of Dox-PVA-ZnO and Dox-PVA-ZnO/CdO, respectively. However, Dox-PVA–Ni-ZnO/CdO produced only 20% cell viability, significantly less than ($p<0.05$) obtained by Dox alone and unloaded nanoparticles alone at the same concentration. Loading Dox to ZnO nanoparticles may increase the Dox cellular uptake by endocytosis [34]. Moreover, a combination between Dox and ZnO nanoparticles may increase the sensitivity of cells to Dox and hence, enhance cell death [35].

The higher toxicity obtained by Ni-doped nanoparticles could be explained in the light of the results of *in vitro* release and encapsulation efficiency. Ni-ZnO/CdO showed about 100 % EE, which means more Dox molecules are available on the nanoparticle surface. Moreover, Ni-doped nanoparticles provided a more sustained and controlled release of Dox so that the drug could exert its effect over a longer period. On the contrary, ZnO and ZnO/CdO provided faster drug release, associated with rapid drug efflux.

4. Conclusions

Magnetic Ni-doped ZnO/CdO nanocomposite and individual nanomaterials (ZnO, CdO, ZnO/CdO) have been successfully synthesized by a green method using BRHE. The prepared nanomaterials' structural, crystalline, optical, and surface properties have been determined using several characterization methods. The anticancer activity of pure and Dox-loaded PVA coated nanomaterials has been used as an anticancer drug against HEPG2 cells as a model of human cancerous cells. PVA-coated Ni-ZnO/CdO was the best carrier for Dox among the tested nanoparticles as it produced the highest E.E%, the more sustained release, and the highest cytotoxicity. These novel nanocarriers need to be studied more deeply on animal models or in clinical investigations in future work.

Funding

This research received no external funding.

Acknowledgments

The authors acknowledge the National Institute of Laser Enhanced Sciences- Cairo University and the National Research Center for supporting this work.

Conflicts of Interest

The authors declare no conflict of interest.

References

1. Singh, K.R.B.; Nayak, V.; Singh, J.; Singh, A.K.; Singh, R.P. Potentialities of bioinspired metal and metal oxide nanoparticles in biomedical sciences. *RSC Adv.* **2021**, *11*, 24722-24746, https://doi.org/10.1039/D1RA04273D.
2. Naseem, T.; Durrani, T. The role of some important metal oxide nanoparticles for wastewater and antibacterial applications: A review. *Environmental Chemistry and Ecotoxicology* **2021**, *3*, 59-75, https://doi.org/10.1016/j.enceco.2020.12.001.
3. Anjum, S.; Hashim, M.; Malik, S.A.; Khan, M.; Lorenzo, J.M.; Abbasi, B.H.; Hano, C. Recent Advances in Zinc Oxide Nanoparticles (ZnO NPs) for Cancer Diagnosis, Target Drug Delivery, and Treatment. *Cancers* **2021**, *13*, 4570, https://doi.org/10.3390/cancers13184570.
4. Skheel, A.Z.; Muneer H.J.; Abd, A.N. Green synthesis of cadmium oxide nanoparticles for biomedical applications (antibacterial, and anticancer activities). *Materials Today: Proceedings* **2021**, *45*, 5793-5799, https://doi.org/10.1016/j.matpr.2021.03.168.
5. Fatima, H.; Charinpanitkul, T.; Kim, K.-S. Fundamentals to Apply Magnetic Nanoparticles for Hyperthermia Therapy. *Nanomaterials* **2021**, *11*, 1203, https://doi.org/10.3390/nano11051203.
6. Stueber, D.D.; Villanova, J.; Aponte, I.; Xiao, Z.; Colvin, V.L. Magnetic Nanoparticles in Biology and Medicine: Past, Present, and Future Trends. *Pharmaceutics* **2021**, *13*, 943, https://doi.org/10.3390/pharmaceutics13070943.
7. Mannu, R.; Karthikeyan, V.; Velu, N.; Arumugam, C.; Roy, V.A.L.; Gopalan, A.-I.; Saianand, G.; Sonar, P.; Lee, K.-P.; Kim, W.-J.; Lee, D.-E.; Kannan, V. Polyethylene Glycol Coated Magnetic Nanoparticles: Hybrid Nanofluid Formulation, Properties and Drug Delivery Prospects. *Nanomaterials* **2021**, *11*, 440, https://doi.org/10.3390/nano11020440.
8. Norouzi, M.; Yathindranath, V.; Thliveris, J.A. *et al*. Doxorubicin-loaded iron oxide nanoparticles for glioblastoma therapy: a combinational approach for enhanced delivery of nanoparticles. *Sci. Rep*. **2020**, *10*, 11292, https://doi.org/10.1038/s41598-020-68017-y.
9. Li, R.-N. *et al.* Functionalized magnetic nanoparticles for drug delivery in tumor therapy. *Chinese Phys. B* **2021**, *30*, 017502, https://doi.org/10.1088/1674-1056/abb3e6.
10. Mohamed, H.H.; Alomair, N.A.; Akhtar, S.; Youssef, T.E. Eco-friendly synthesized α-Fe_2O_3/TiO_2 heterojunction with enhanced visible light photocatalytic activity. *Journal of Photochemistry and Photobiology A: Chemistry* **2019**, *382*, 111951, https://doi.org/10.1016/j.jphotochem.2019.111951.
11. Mohamed, H.H.; Al Qarni, F.; Alomair, N.A. Design of porous Ga doped TiO_2 nanostructure for enhanced solar light photocatalytic applications. *Materials Research Bulletin* **2021**, *133*, 111057, https://doi.org/10.1016/j.materresbull.2020.111057.
12. Al Qarni, F.; Alomair, N.A.; Mohamed, H.H. Environment-Friendly Nanoporous Titanium Dioxide with Enhanced Photocatalytic Activity. *Catalysts* **2019**, *9*, 799, https://doi.org/10.3390/catal9100799.
13. Mahmoudi, M.; Simchi, A.; Imani, M. *et al.* New approach for the *in vitro* identification of the cytotoxicity of superparamagnetic iron oxide nanoparticles. *Colloids Surf B: Biointerfaces* **2010**, *75*, 300-309, https://doi.org/10.1016/j.colsurfb.2009.08.044.
14. Shah, S.; Chandra, A.; Kaur, A.; Sabnis, N.; Lacko, A.; Gryczynski, Z.R.; Fudala, R.; Gryczynski, I. Fluorescence properties of doxorubicin in PBS buffer and PVA films. *J. Photochem. Photobiol. B: Biology* **2017**, *170*, 65-69, https://doi.org/10.1016/j.jphotobiol.2017.03.024.
15. Plichta, Z.; Kozak, Y.; Panchuk, R.; Sokolova, V.; Epple, M.; Kobylinska, L.; Jendelová, P.; Horák, D. Cytotoxicity of doxorubicin-conjugated poly[N-(2-hydroxypropyl)methacrylamide]-modifiedγ-Fe_2O_3 nanoparticles towards human tumor cells. *Beilstein J Nanotechnol* **2018**, *9*, 2533-2545, https://doi.org/10.3762/bjnano.9.236.

16. Ramnandan, D.; Mokhosi, S.; Daniels, A.; Singh, M. Chitosan, Polyethylene Glycol and Polyvinyl Alcohol Modified $MgFe_2O_4$ Ferrite Magnetic Nanoparticles in Doxorubicin Delivery: A Comparative Study *In vitro*. *Molecules* **2021**, *26*, 3893, https://doi.org/10.3390/molecules26133893.
17. Prabha, G.; Raj, V. Sodium alginate-polyvinyl alcohol-bovin serum albumin coated Fe_3O_4 nanoparticles as anticancer drug delivery vehicle: Doxorubicin loading and *in vitro* release study and cytotoxicity to HepG2 and L02 cells. *Mater Sci and Eng: C* **2017**, *79*, 410-422, https://doi.org/10.1016/j.msec.2017.04.075.
18. Butsat, S.; Siriamornpun, S. Antioxidant capacities and phenolic compounds of the husk, bran and endosperm of Thai rice. *Food Chemistry* **2010**, *119*, 606-613, https://doi.org/10.1016/j.foodchem.2009.07.001.
19. Goufo, P.; Trindade, H. Rice antioxidants: phenolic acids, flavonoids, anthocyanins, proanthocyanidins, tocopherols, tocotrienols, γ-oryzanol, and phytic acid. *Food Science and Nutrition* **2014**, *2*, 75-104, https://doi.org/10.1002/fsn3.86.
20. Mohamed, H.H. Sonochemical synthesis of ZnO hollow microstructure/reduced graphene oxide for enhanced sunlight photocatalytic degradation of organic pollutants. *J. Photochem. Photobiol A: Chemistry* **2018**, *353*, 401-408, https://doi.org/10.1016/j.jphotochem.2017.11.052.
21. Mohamed, H.H.; Alsanea, A.A.; Alomair, N.A. *et al*. ZnO@ porous graphite nanocomposite from waste for superior photocatalytic activity. *Environ Sci Pollut Res* **2019**, *26*, 12288-12301, https://doi.org/10.1007/s11356-019-04684-3.
22. Fall, A.; Sackey, J.; Mayedwa, N.; Ngom, B.D. Investigation of structural and optical properties of CdO nanoparticles via peel of Citrus x sinensis. *Materials Today: Proceedings* **2021**, *36*, 298-302, https://doi.org/10.1016/j.matpr.2020.04.057.
23. Arshad, M.; Azam, A.; Ahmed, A.S.; Mollah, S.; Naqvi, A.H. Effect of Co substitution on the structural and optical properties of ZnO nanoparticles synthesized by sol-gel route. *J. of Alloys and Comp.* **2011**, *509*, 8378-8381, https://doi.org/10.1016/j.jallcom.2011.05.047.
24. Guglieri, C.; Céspedes, E.; Espinosa, A. *et. al*. Evidence of Oxygen Ferromagnetism in ZnO Based Materials. *Adv. Funct. Mat* **2014**, *24*, 2094-2100, https://doi.org/10.1002/adfm.201303087.
25. Lungu, I.I.; Grumezescu, A.M.; Fleaca, C. Unexpected Ferromagnetism—A Review. *Appl. Sci.* **2021**, *11*, 6707, https://doi.org/10.3390/app11156707.
26. Akhil, K.; Jayakumar, J.; Gayathri, G.; Khan, S.S. Effect of various capping agents on photocatalytic, antibacterial and antibiofilm activities of ZnO nanoparticles. *J. Photochem. Photobiol. B: Biology* **2016**, *160*, 32-42, https://doi.org/10.1016/j.jphotobiol.2016.03.015.
27. Liu, J.; Ma, X.; Jin, S.; Xue, X.; Zhang, C.; Wei, T.; Guo, W.; Liang, X.J. Zinc Oxide Nanoparticles as Adjuvant to Facilitate Doxorubicin Intracellular Accumulation and Visualize pH-Responsive Release for Overcoming Drug Resistance. *Mol Pharm.* **2016**, *13*, 1723-1730, https://doi.org/10.1021/acs.molpharmaceut.6b00311.
28. Coates, J. Interpretation of Infrared Spectra: A Practical Approach. *In: Meyers, R.A., Ed., Encyclopedia of Analytical Chemistry* **2000**, John Wiley & Sons Ltd., Chichester.
29. Pereira, P.; Serra, A.C.; Coelho, J.F.J. Vinyl Polymer-based technologies towards the efficient delivery of chemotherapeutic drugs. *Progress in Polymer Science* **2021**, *121*, 101432, https://doi.org/10.1016/j.progpolymsci.2021.101432.
30. Nigam, S.; Barick, K.C.; Bahadur, D. Development of citrate-stabilized Fe_3O_4 nanoparticles: Conjugation and release of doxorubicin for therapeutic applications. *Journal of Magnetism and Magnetic Materials* **2011**, *323*, 237-243, https://doi.org/10.1016/j.jmmm.2010.09.009.
31. Sharma, H.; Kumar, K.; Choudhary, C.; Mishra, P.K.; Vaidya, B. Development and characterization of metal oxide nanoparticles for the delivery of anticancer drug. *Artif Cells Nanomed Biotechnol*. **2016**, *44*, 672-679, https://doi.org/10.3109/21691401.2014.978980.
32. Akhtar, M.; Ahamed, M.; Kumar, S.; Khan, M.M.; Ahmad, J.; Alrokayan, A.S. Zinc oxide nanoparticles selectively induce apoptosis in human cancer cells through reactive oxygen species. *Int J Nanomedicine* **2012**, *7*, 845-857, https://doi.org/10.2147/IJN.S29129.
33. Renu, K.; Abilash, V.G.; Tirupathi Pichiah, P.B.; Arunachalam, S. Molecular mechanism of doxorubicin-induced cardiomyopathy - An update. *Eur J Pharmacol.* **2018**, *818*, 241-253, https://doi.org/10.1016/j.ejphar.2017.10.043.
34. Ortiz-Casas, B.; Galdámez-Martínez, A.; Gutiérrez-Flores, J. *et.al.* Bio-acceptable 0D and 1D ZnO nanostructures for cancer diagnostics and treatment. *Materials Today* **2021**, *50*, 533-569, https://doi.org/10.1016/j.mattod.2021.07.025.

35. Batool, M.; Khurshid, S.; Daoush, W.M.; Siddique, S.A.; Nadeem, T. Green Synthesis and Biomedical Applications of ZnO Nanoparticles: Role of PEGylated-ZnO Nanoparticles as Doxorubicin Drug Carrier against MDA-MB-231(TNBC) Cells Line. *Crystals* **2021**, *11*, 344, https://doi.org/10.3390/cryst11040344.